Computational Condensed Matter 45 (2025) e01175

Contents lists available at ScienceDirect

Computational Condensed Matter

journal homepage: www.elsevier.com/locate/cocom

Computational analysis of hydrogen storage and physical behavior of Al, Ga, and In-based Copper hydrides

R.M. Tanvir [a,b], S. Tanvir [a,b], Md Al-Amin [a,b], A. Rayhan [c], S. Mahmud [a,b,*]

[a] Smart Computing Research Laboratory (SCRL), Department of EEE, Jatiya Kabi Kazi Nazrul Islam University, Mymensingh, 2224, Bangladesh
[b] Department of EEE, Jatiya Kabi Kazi Nazrul Islam University, Mymensingh, 2224, Bangladesh
[c] Department of Arts and Science, Bangladesh Army University of Science and Technology (BAUST), Sayadpur, Bangladesh

ARTICLE INFO

Keywords:
DFT
Wien2k
Stability
Metal
Hydrogen storage

ABSTRACT

Hydrogen is a promising clean energy carrier due to its high gravimetric energy density and decarbonization potential. This study investigates the structural, mechanical, electronic, and hydrogen storage properties of $XCuH_3$ (X = Al, Ga, In) hydrides using first-principles calculations. The optimized lattice constants are 3.50, 3.56, and 3.69 Å, corresponding to hydrogen storage capacities of 3.23, 2.22, and 1.67 wt% for $AlCuH_3$, $GaCuH_3$, and $InCuH_3$, respectively. $AlCuH_3$ demonstrates superior mechanical strength, thermal stability, and strong interatomic bonding, supported by its highest Debye temperature, bulk, shear, and Young's moduli. In contrast, $InCuH_3$ exhibits the greatest ductility with high Pugh's ratio, and pronounced elastic anisotropy, while $GaCuH_3$ shows intermediate properties. Band structure and density of states confirm metallic behavior, whereas Poisson's ratio highlights the ionic bonding contribution. Overall, these insights enhance the understanding of $XCuH_3$ hydrides, guiding their potential applications in hydrogen storage and energy technologies.

1. Introduction

Fossil fuels have long dominated global energy sources, but their environmental impact, among others contributions to climate change and global warming, has raised noteworthy concerns [1–4]. They are not only non-renewable and costly but also release harmful gases, chemicals, and heat upon combustion, exacerbating environmental degradation [5–7]. With the continuous rise in global energy demand and the simultaneous depletion of fossil fuel reserves, the need for sustainable alternatives has become urgent [8]. This challenge has stimulated research into clean energy options, including renewables, hydrogen power, and nuclear energy [9]. Among these alternatives, hydrogen energy stands out as a particularly promising candidate due to its high energy density and clean combustion profile, producing only water as a byproduct. It is not only toxicity free element, but also operates independently of weather conditions, unlike some renewables, and originates no nuclear waste [10,11]. For these advantages, it has potential as a fuel for households, vehicles, and portable electronic devices [12]. Though it has several advantages over other fuels in particular industries, there are many obstacles if we try to implement it as a notable energy source [13–15]. A major challenge stands in creating effective ways to store hydrogen, which is crucial for its real-world use and requires substantial technological advancements [16,17]. Most ongoing research is focused on designing compact and efficient hydrogen storage systems suitable for applications in industry, homes, transportation, and energy production [18–20]. For scientific applications, the stability of a material is one of the most significant parameters. Material stability can be evaluated by calculating elastic constants, either through computational methods or using the empirical pseudopotential approach within the virtual crystal approximation [21–25]. Research has been carried out for quite a while to evaluate the feasibility of various materials, including metals, complex hydrides, metal-organic frameworks (MOFs), carbonaceous materials, and zeolites, for hydrogen storage applications [26–32]. At present, hydrogen is primarily stored using three main techniques: as a gas, as a liquid, or in solid-state form [16]. Cubic perovskite hydrides (ABH_3) are currently being explored as promising candidates for solid-state hydrogen storage [33]. Scientific interest in ABH_3 perovskite-type hydrides has grown significantly, with research increasingly relying on both experimental and theoretical approaches [34–36]. ABH_3 compounds generally exhibit gravimetric hydrogen densities ranging between 1.2 wt% and 6 wt% [37,38]. Recently, ABH_3 compounds containing alkali and alkaline earth metals have been

* Corresponding author. Smart Computing Research Laboratory (SCRL), Department of EEE, Jatiya Kabi Kazi Nazrul Islam University, Mymensingh, 2224, Bangladesh.
E-mail address: shuaib.eee.iu@gmail.com (S. Mahmud).

https://doi.org/10.1016/j.cocom.2025.e01175
Received 18 September 2025; Received in revised form 6 November 2025; Accepted 16 November 2025
Available online 17 November 2025
2352-2143/© 2025 Elsevier B.V. All rights are reserved, including those for text and data mining, AI training, and similar technologies.

investigated for their potential in hydrogen storage applications [39, 40]. Metal hydride perovskite gives us several advantages over traditional methods of hydrogen storage, such as liquid tanks and compressed gas cylinders. Materials that cannot only acquire high hydrogen content but also remain stable in high concentration are particularly exciting for both theoretical and applied researchers, as this offers a stable solution to hydrogen fuel storage and potential carbon-based fuel replacement [41]. Metallic hydrides are considered favorable for hydrogen storage due to their simple structures, high gravimetric hydrogen capacity, and superior volumetric storage density [42,43]. These hydrides have strong thermodynamic stability along with better kinetics [44]. Also, metal hydride perovskites are considered a safer option for storing hydrogen fuel compared to compressed gas or liquid hydrogen [45]. Discovering new materials with the right combination of crystal structures is essential to reach that goal. Currently, first-principles calculations based on Density Functional Theory (DFT) are a powerful tool to study the physical properties of new materials [46] exhibiting potential for hydrogen storage applications [47]. Recent DFT studies on $LiBH_3$ (B = Cu, Zn, Cd) [36], $GaXH_3$(X = Si, Ge) [7], $NaBH_3$ (B = Cu, Zn, Cd) [11], and $XLiH_3$ (X = Mg, Ca, Sr, and Ba) [25] reveal hydrogen storage capacities of 2.03–8.76 wt%. The Cu-based hydrides $XCuH_3$ (X = Ca and Sr) were investigated by Bilal Ahmed and his co-workers for hydrogen storage applications [48]. The detailed analysis shows that the gravimetric hydrogen storage capacity for $CaCuH_3$ is 2.85 % and $SrCuH_3$ is 1.97 %. By first principal calculation the gravimetric hydrogen storage for $KSrH_3$ (2.33 %), $RbSrH_3$ (1.71 %), $RbGaH_3$ (2.5 %), $CsGaH_3$ (2.0 %), $FrGaH_3$ (2.1 %), $CoCuH_3$ (2.28 %), $NiCuH_3$ (3.0 %), $ZnCuH_3$ (2.7 %), $CsBH_3$ (2.19 %), $RbBH_3$ (3.01 %) also been calculated in literature. From these, we have been inspired for our work to investigate the hydrides for their identical unique characteristics. We investigated the structural, mechanical, electrical, optical, and hydrogen storage capacity characteristics of $XCuH_3$ (X = Al, Ga, In) in this article. This represents the first comprehensive study of perovskite-type hydrides to the best of the authors' knowledge. There are no theoretical or experimental investigations related to different physical properties presented in this study. The information presented in this article can be useful for future studies and serve as a reference, aiding in synthesis. Four sections make up this research paper. In the second section, the computational methodology of this research is summarized. The third section describes the full results and discussion of all properties, and the conclusion throughout the research is summarized in section four.

2. Methodology

The density functional theory (DFT) architecture built within the Wien2k program is used to carry out the calculation procedures [49]. Computation details: The unit cell geometry of the Cu–Group 13 hydride gradient series was optimized using the GGA-PBE functional. By creating the crystal arrangement in Wien2k, we laid the foundation for a thorough investigation of physical properties using the Kohn-Sham equation. In order to provide a solid foundation for further research, the fundamental state variables were first carefully determined using the Generalized Gradient Approximation (GGA) Perdew–Burke–Ernzerhof (PBE) technique. As the structural basis, we used the full-potential linearized augmented plane wave (FP-LAPW) method with all geometric characteristics fine-tuned within the third-order Birch–Murnaghan equation, as well as the TB-mBJ (Tran–-Blaha–modified Becke–Johnson) method to systematically tailor opto-electronic bandgap, ensuring adherence to experimental data while maintaining mathematical rigor. The lattice of 1000 k-points was artistically arranged in a $10 \times 10 \times 10$ matrix, the $R_{MT} \times K_{Max}$ value was set at 6.5, the charge convergence was adjusted to a strict 10^{-5} Ry, the energy merging was meticulously balanced at 0.001 eV, and the G_{MAX} creating was raised to 10, creating a unique the basis to begin the mathematical voyage [50]. We used the electron valence configurations *s-p* for Al, *s* for H, *s-p-d* for Cu, and a flexible *s-p-d* arrangement for both Ga and In for this computation. By consistently applying these carefully chosen selection criteria in our computer model, we significantly improve the clarity and effectiveness of the identified material properties of our molecules.

3. Results and discussion

3.1. Structural properties

The metal hydrides $XCuH_3$ (X = Al, Ga, In) are simple cubic with a space group of Pm3m (221 no). The unit cell of $XCuH_3$ contains five atoms. In the crystal structure, Al, Ga, and In atoms are positioned at (0, 0, 0), Cu at (0.5, 0.5, 0.5), and three Hydrogen atoms at (0.5, 0.5, 0), (0, 0.5, 0.5), (0.5, 0, 0.5). The energy-volume optimization curves of $XCuH_3$ are obtained by the Birch–Murnaghan equation of state. The lattice constant for the $XCuH_3$ compounds is given as follows: $AlCuH_3$ (3.50 Å), $GaCuH_3$ (3.56 Å), and $InCuH_3$ (3.69 Å). The unit cell configurations of $XCuH_3$ for the individual cation substitutions are shown in Fig. 1. We can see that with the increase of atomic number of X, the lattice constant of $XCuH_3$ adventures a progressive increase. Al, Ga, and In are elements of group 13 and In has a higher atomic mass than Al and Ga whereas the atomic mass of Ga > Al. Therefore, it is clear that the lattice constant increases with their atomic mass.

The tolerance factor (t_G) can be calculated by the following formula, which has a crucial rule for understanding structural stability [51].

$$t_G = \frac{(R_X + R_H)}{\sqrt{2}(R_{Cu} + R_H)} \tag{1}$$

In this equation, R_X, R_{Cu}, and R_H mean the ionic radius of X (Al, Ga, In), Cu, and H atoms. The tolerance factor stability for a cubic structure is 0.75 and 1.05 [52]. From this equation, we can find the tolerance factors of $AlCuH_3$, $GaCuH_3$, and $InCuH_3$ perovskites are 0.98, 1.00, and 1.02, respectively. From these values, we can say that $XCuH_3$ compounds meet the conditions for structural stability and for forming cubic perovskites. Stable cubic perovskite structure provides a robust host scheme, avoiding phase decomposition and ensuring consistent performance.

To know that our material is thermodynamically stable, we need to calculate the formation energy. Thermodynamic stability describes the energy state of a compound relative to its constituent elements and any alternative products or reactants it could form. For thermodynamic stability, a material formation energy value needs to be negative, indicating that the compound energetically prefers to remain intact rather than break down into its elemental components or react with other materials. This formation energy can be calculated by the following formula [53–58]:

$$\Delta E_F = \left(E_F(XCuH_3) - E(X) - E(Cu) - \frac{3}{2}E(H_2) \right) \tag{2}$$

Here in this equation, $E_F\,(XCuH_3)$ is the total energy of $XCuH_3$. $E(X)$, $E(Cu)$, and $E(H_2)$ indicate the total individual energy of X (Al, Ga, and In), Copper (Cu), and H_2 (Hydrogen). From Table 1, we see that the formation energy of $AlCuH_3$, $GaCuH_3$, and $InCuH_3$ is −1.62, −1.68, and −1.76 eV/atom, respectively. As we find the value of formation energies is all negative, these materials are thermodynamically stable. Importantly, formation energies are relatively moderate, so hydrogen desorption may be a low-energy process, which places these materials as promising candidates for reversible hydrogen storage at intermediate temperatures.

3.2. Phonon properties

The number of vibrational modes in phonons is directly related to the number of atoms in a crystal's cell. This results for the investigated hydrogen compounds with a quintet of atoms per cell in a total of 15 modes, derived of the mater constraint 3 times atom number [59,60].

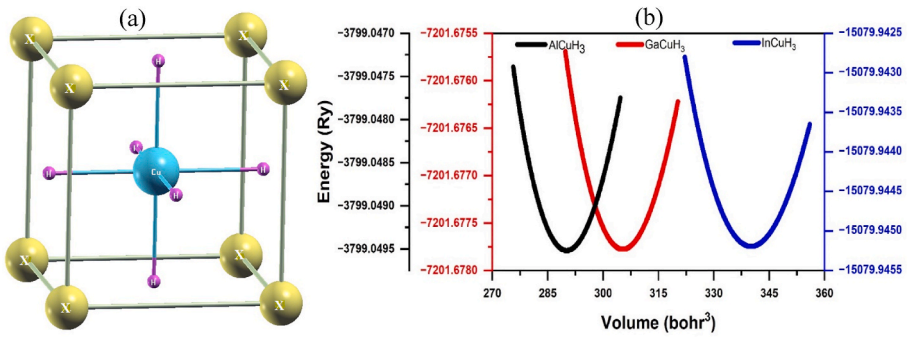

Fig. 1. (a) Unit cell and **(b)** Energy-Volume optimization curve of $XCuH_3$ (X = Al, Ga, and In).

Table 1
The optimized cubic lattice constant (a_0), volume (V_0), tolerance factor (t_G), and formation energy (ΔE_F) of $XCuH_3$.

Hydrides	a_0 (Å)	V_0 (bohr^3)	t_g	ΔE_F (eV/atom)
$AlCuH_3$	3.50	290.08	0.98	−1.62
$GaCuH_3$	3.56	305.53	1.00	−1.68
$InCuH_3$	3.69	340.16	1.02	−1.76

Among these, three of the modes are acoustic phonons and $3N-3$ modes are optical phonons [61,62]. Phonon dispersion curves along the high-symmetry directions X–R–M–Γ–R in the Brillouin zone. The calculated phonon dispersion relations $AlCuH_3$, $GaCuH_3$, and $InCuH_3$ are illustrated in Fig. 2(a–c). The absence of significant imaginary frequencies in the Brillouin zone, confirms their dynamical stability [63–65]. A very small imaginary frequency (<-2 cm^{-1}) in the $AlCuH_3$ phonon spectrum, however we note that this can generally be ignored as it falls within numerical uncertainty.

3.3. Electronic properties

The band structure and density of states are essentially the main features when we look at the electronic properties of a material [66]. Total density of states (TDOS) and partial density of states (PDOS) are helpful descriptors of electronic band structure, providing insight into how atomic exchange and relaxation may influence band structure for a given compound [67]. Fig. 3 displays the electronic band structure of $AlCuH_3$, $GaCuH_3$, and $InCuH_3$.

From the three-band structure, at 0 eV, the red line represents the Fermi level. The lower part of Fermi level is valence band, and the upper part of fermi level is conduction band. The band gap (or energy gap in terms of the electronic band structure of a solid) is the range of energies in a solid, semiconductor, or insulator, where no electronic states can exist, or equivalently, the energy difference between the top of the valence band and the bottom of the conduction band. But in these three materials, no such state exists, hence there is no band gap between them since there is no band gap between the valence band and the conduction band, which is usually seen in semiconductors and insulators; these materials are metallic. So, we can say that $XCuH_3$ has very good electrical conductivity and increases the efficient charge transfer in hydrides during hydrogen storage and release. In Table 2, the band gaps of $XCuH_3$ are summarized and compared against representative literature data.

The density of states describes how many energy states are available that an electron can occupy within a system. In Fig. 4, the total DOS and

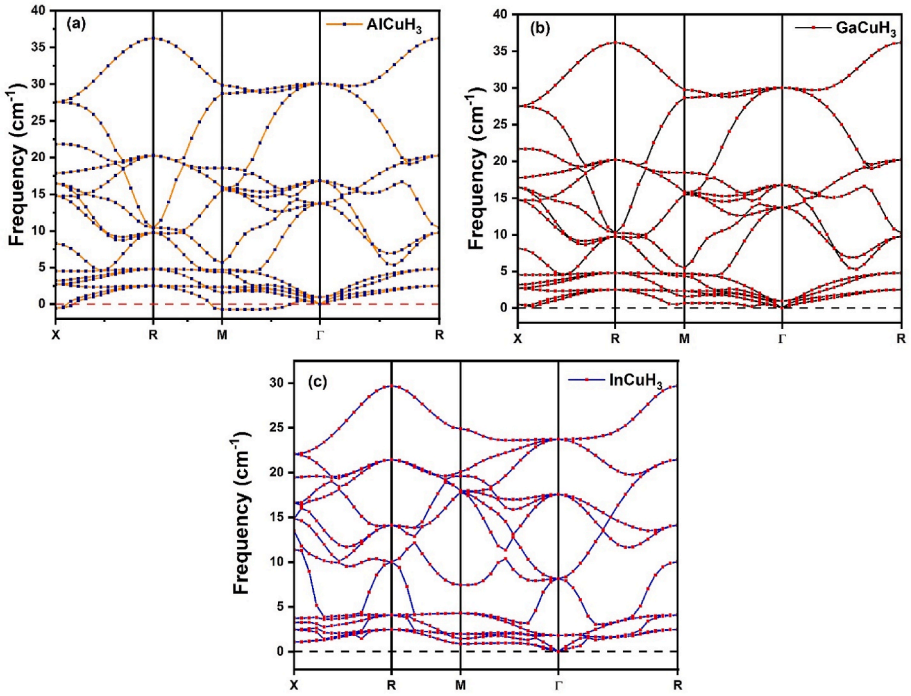

Fig. 2. Calculated phonon dispersion curves of **(a)** $AlCuH_3$ **(b)** $GaCuH_3$ and **(c)** $InCuH_3$.

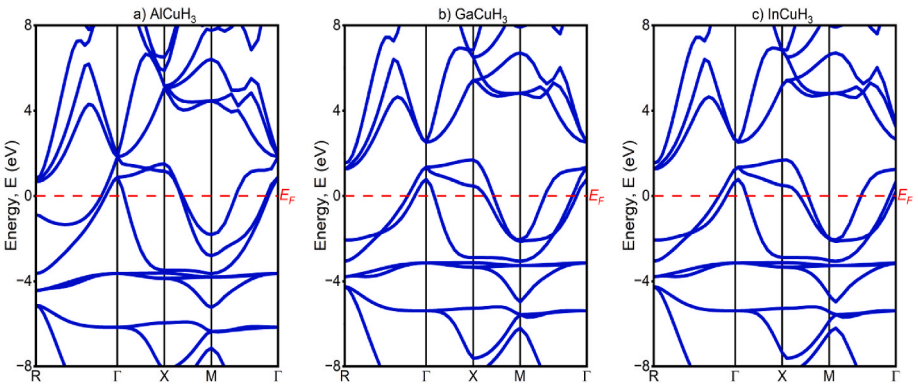

Fig. 3. (a) Band structure of $AlCuH_3$, **(b)** $GaCuH_3$ and **(c)** $InCuH_3$.

Table 2
Band Gap, and lattice Parameters for $XCuH_3$ (X = Al, Ga, In) and other Hydride materials.

Compounds	Lattice Parameter	E_g (eV)	References
$AlCuH_3$	3.50	0.00	Present study
$GaCuH_3$	3.56	0.00	Present study
$InCuH_3$	3.69	0.00	Present study
$NaCrH_3$	3.54	0.00	[68]
$KCrH_3$	3.74	0.00	[68]
$KGaH_3$	–	0.00	[69]
$LiGaH_3$	–	0.00	[69]
$CaNiH_3$	3.55	0.00	[70]
$CaMnH_3$	3.60	0.00	[71]
$CaCoH_3$	3.48	0.00	[71]
$CaFeH_3$	3.50	0.00	[71]
$KScH_3$	4.19	0.00	[72]
$NaScH_3$	4.07	0.00	[72]
$MgCrH_3$	3.46	0.00	[73]
$CrRuH_3$	4.00	0.00	[74]
$VRuH_3$	3.92	0.00	[74]
$NiRuH_3$	3.99	0.00	[74]
$MgSiH_3$	3.98	0.00	[75]
$MgCoH_3$	3.32	0.00	[76]
$MgNiH_3$	3.36	0.00	[76]
$MgCuH_3$	3.49	0.00	[76]

partial DOS (TDOS and PDOS) are illustrated for various orbitals in $XCuH_3$. It is an effective way to assess how each state contributes to the overall electronic band structure by analyzing the density of states (DOS) curves. The highest TDOS values of $AlCuH_3$, $GaCuH_3$, and $InCuH_3$ at the Fermi level, are 0.92 electrons/eV, 1.00 electrons/eV, and1.15 electrons/eV. Though the peak value of $AlCuH_3$ shows a value of 9.79 electrons/eV at −3.75 eV, while $GaCuH_3$ indicates the peak value of 8.59 electrons/eV at −3.45 eV, and $InCuH_3$ shows the peak value of 9.73 electrons/eV at −3.18 eV. TDOS provides an overview of the electronic states available at each energy level, but PDOS allows the decomposition of the total DOS into atomic and orbital contributions (e.g., *s*, *p*, and *d* orbitals from specific elements) in $AlCuH_3$, between −8 and −3 eV, Cu *d*-state and H *s*-state contributes significantly to the valence band, whereas from −3 to 0 eV Al s-state contribute significantly to the valence band. In the conduction band *p*-states of Al dominant contributor. Al and H *s*-state has minimal contribution in this range. In $GaCuH_3$, between −8 and −3 eV, the Cu *d* and H *s*-state contribute significantly on the valence band, and Ga *d*-state contribute little range. Ga *d*-state has the greatest influence to the valence band, which ranges from −3 to 0 eV. In the conduction band *p*-states of Ga clearly the primary contributor, and Ga *d*-state and H *s*-state contributes little to the conduction band. In $InCuH_3$, between −8 and −3 eV, the Cu *d*-state and H s-state are heavily involved in the formation of the valence band, and In d-state contributes significantly to the valence band. While the H *s*-state plays a very small role in this energy range, the *p*-states of In contribute more, the *d*-states of In,

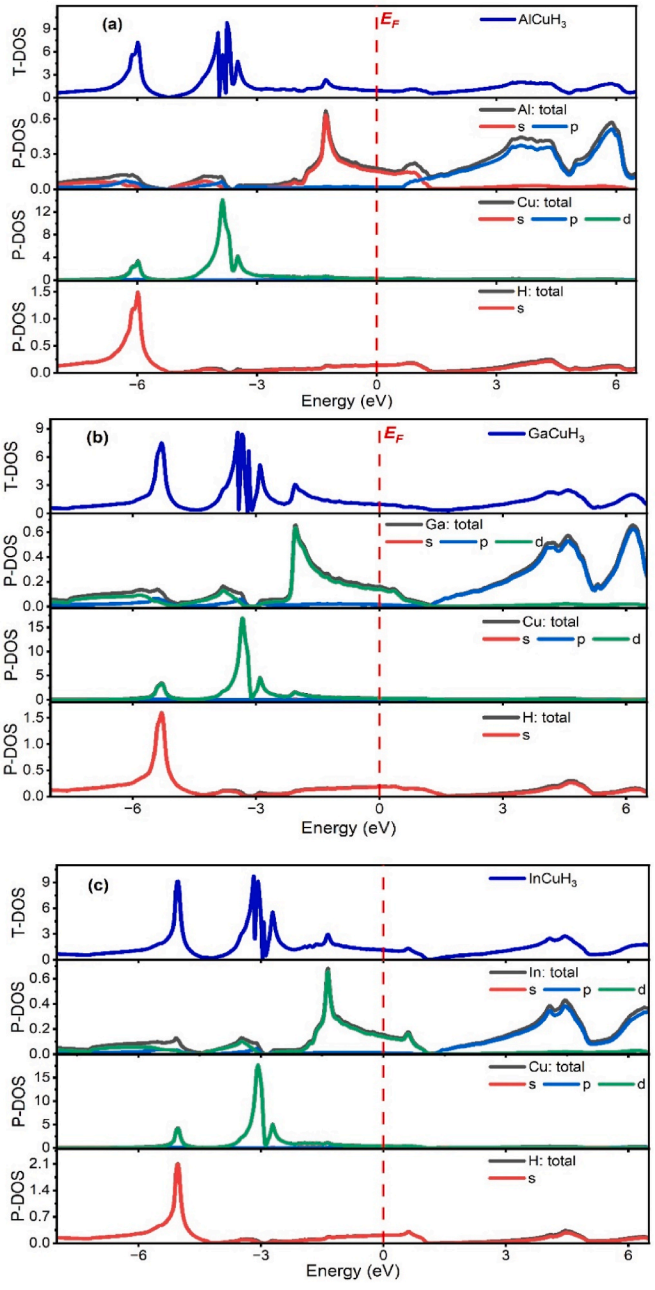

Fig. 4. TDOS and PDOS of **(a)** $AlCuH_3$, **(b)** $GaCuH_3$ and **(c)** $InCuH_3$ hydrides.

and the *s*-state of H contribute little in this conduction band. Finally, we said that the TDOS for $AlCuH_3$, $GaCuH_3$, and $InCuH_3$ cross E_F, providing evidence of their metallic properties.

3.4. Optical properties

Optical properties of a material are extremely necessary for gaining knowledge into their behavior when they are exposed to light, basically how it absorbs, reflects, refracts, or scatters electromagnetic radiation (especially in the visible, infrared, or ultraviolet ranges). Materials with specific optical absorption characteristics are crucial in photochemical hydrogen storage systems, where exposure to light triggers the uptake or release of hydrogen [77]. Furthermore, analyzing the optical response of these materials helps forecast how they will behave under various lighting conditions, which is especially important for managing heat during hydrogen storage, particularly when sunlight is involved. To determine the optical properties of the studied materials, the dielectric function and other frequency-dependent optical properties are calculated. From the various properties of a material, the dielectric function should be considered first, and it is essential. The dielectric function has two parts: the Real dielectric and the Imaginary dielectric. The equation for the dielectric function is [78]:

$$\varepsilon_1(\omega) = \varepsilon_1(\omega) + i\varepsilon_2(\omega) \tag{3}$$

For incoming electromagnetic radiation in the material, there is some dispersion and polarization processes occur, which can be investigated by the fundamental component of the dielectric function and the imaginary component of the dielectric function. We can determine the absorption of the material's internal structure [79,80].

Fig. 5(a) shows the graph for the real part of the dielectric function, which is determined by the following equations [81]:

$$\varepsilon_1(\omega) = 1 + \frac{2p}{\pi} \int_0^{\infty} \frac{\omega' \varepsilon 2(\omega')}{\omega'^2 - \omega^2} \, d\omega \tag{4}$$

From this graph, it is clear that $AlCuH_3$, $GaCuH_3$, and $InCuH_3$ have static values of 30.08, 24.06, and 48.92, respectively. The value of real dielectric function goes to the negative zone at 3.06 eV for $AlCuH_3$, 0.97 eV for $GaCuH_3$ and 3.96 eV for $InCuH_3$, respectively. A negative value in $\varepsilon_1(\omega)$ response signifies strong surface reflection at the material, which leads to reduced light transmission [82] and the peak values of $\varepsilon_1(\omega)$ for studied materials are 31.51, 28.09, and 48.92, respectively. At high energy levels, there is a noticeable difference in energy for the differences in $\varepsilon_1(\omega)$ values for three compounds.

Fig. 5(b) shows a graph of the imaginary dielectric function by which we can know the absorbing capabilities of these three compounds. The static values of Imaginary dielectric $\varepsilon_2(\omega)$ for $AlCuH_3$, $GaCuH_3$, and $InCuH_3$ are 3.41, 1.96, and 26.26, respectively. For that particular spot, the static value is not zero, hence they have contact between the material surface and the electromagnetic radiation [82]. For $AlCuH_3$, $GaCuH_3$, and $InCuH_3$, the highest values of $\varepsilon_2(\omega)$ are 22.56, 25.56, and 33.64, respectively and these values are found at 0.37, 0.8, and 0.1 eV.

This imaginary part can be calculated by,

$$\varepsilon_2(\omega) = \frac{(h' e^2)}{\pi \omega^2 m^2} \sum_{v,c} \int_{BZ}^{\infty} \left[M_{cv}(k) \right]^2 \delta \left[\omega_{cv}(k) - \omega \right] d^3k \tag{5}$$

The way a material reacts to light photon exposure can be interpreted by using its absorption characteristics [79]. By this, we can find out how efficiently a material can absorb photons or energy packets. Fig. 5(c) displays the absorption properties of these three studied materials. Absorption peak located at 9.95 eV, 10.14 eV, and 9.76 eV for $AlCuH_3$, $GaCuH_3$ and $InCuH_3$, respectively. The absorption values of those energy levels are 138.8×10^4, 145.5×10^4, and 144.5×10^4 cm^{-1}, respectively. These three materials exhibits, respectively, the best ($GaCuH_3$) and the worst ($AlCuH_3$) absorption values. The absorption coefficient is the ratio of the total optical power absorbed to the total optical power incident on the cell surface and low resistivity. Thus, materials can absorb UV light; therefore, they can be attractive for hydrogen storage applications. This absorption coefficient can be calculated by, $\alpha(\omega)$ [83]:

$$\alpha(\omega) = \frac{4\pi K(\omega)}{\lambda} \tag{6}$$

Absorption coefficient having higher value means the electron has a higher energy level above from valence band to the conduction band.

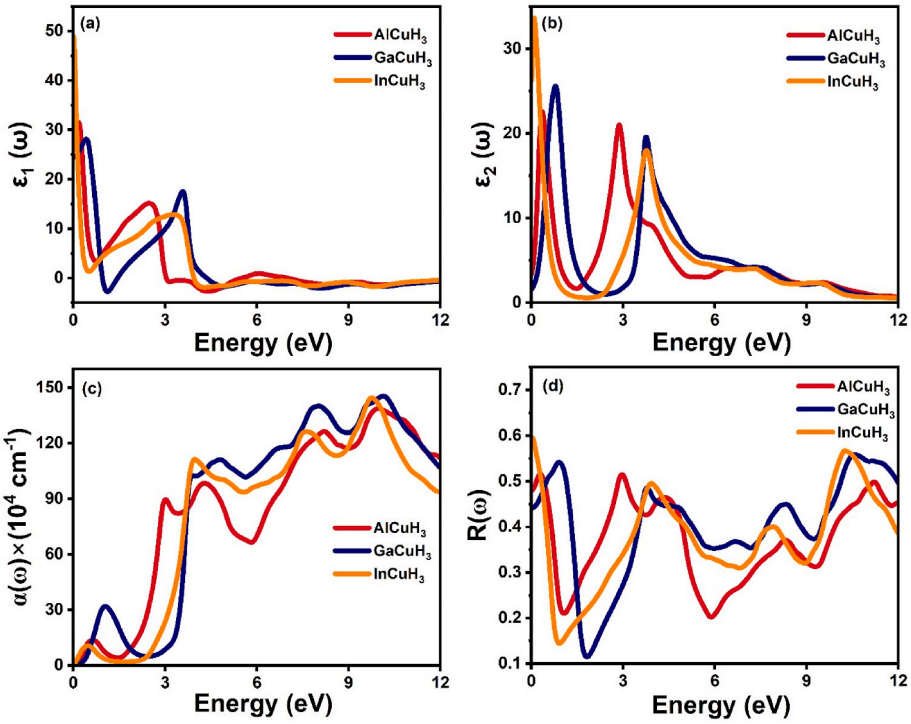

Fig. 5. (a) $\varepsilon_1(\omega)$: Real Dielectric **(b)** $\varepsilon_2(\omega)$: Imaginary dielectric function, **(c)** $\alpha(\omega)$: Absorption coefficient and **(d)** $R(\omega)$: Reflectivity.

The existence of the highest absorption peak in ultraviolet region confirms that these materials are optically active with high absorption intensity. Fig. 5(d) depicts the reflectivity of the $AlCuH_3$, $GaCuH_3$, and $InCuH_3$. Reflectivity describes how much incoming electromagnetic radiation is reflected off the surface of a material [84]. By examining the graph, we can see that the static values are 0.48, 0.44, and 0.59, respectively. $InCuH_3$ show the peak value of reflectivity at 0.4 eV, and the value is 0.594. The reflectivity value of these three materials continuously increases and decreases from start to end. We can find the reflectivity value by using the formula [85]:

$$R(\omega) = \frac{K^2 + (1-n)^2}{K^2 + (1+n)^2} \tag{7}$$

In Fig. 6(a), the refractive index is shown by $n(\omega)$, which is a dimensionless number that is directly related to the speed of light moving through a material and indicates how fast light will propagate through a medium; that is, the amount by which the speed of light is reduced in the medium used. The refractive index can be calculated by:

$$n(\omega) = \left(\frac{\varepsilon_1(\omega)}{2} + \frac{\sqrt{\varepsilon_1^2(\omega) + \varepsilon_1^2(\omega)}}{2} \right)^{\frac{1}{2}} \tag{8}$$

The static values for $AlCuH_3$, $GaCuH_3$, and $InCuH_3$ are found as 5.49, 4.95, and 7.23, respectively. The greatest refractive values for materials are 5.7, 5.43, and 7.23, respectively, and these highest values are found at 0.2 eV, 0.64 eV, and 0.2 eV. After the highest value of refractive index, $n(\omega)$ decreases sharply and then again increases for all three compounds, but after some energy level, it decreases gradually till the end. This larger refractive index leads to a higher degree of polarization, thus improving the hydrogen storage capacity of the material [86,87]. The extinction coefficient $k(\omega)$ is related to the absorption and scattering. It describes how strongly a material can absorb or reflect light at a particular wavelength. This extinction coefficient is given as [88]:

$$k(\omega) = \left(-\frac{\varepsilon_1(\omega)}{2} + \frac{\sqrt{\varepsilon_1^2(\omega) + \varepsilon_1^2(\omega)}}{2} \right)^{\frac{1}{2}} \tag{9}$$

The $k(\omega)$ for $AlCuH_3$, $GaCuH_3$, and $InCuH_3$ is depicted in Fig. 6(b). At the energy of 0 eV, the $k(\omega)$ values are 0.3, 0.16, and 1.82 for the studied materials, respectively. For $AlCuH_3$, 2.96 is the highest extinction value at this energy levels of 2.98 eV, $GaCuH_3$ and $InCuH_3$, 3.21 and 2.92 are the highest extinction values at the energy level of 1.07 eV and 0.39 eV, respectively. The higher extinction coefficient value indicates a stronger absorption tendency [89]. Hence, from these three materials, $GaCuH_3$ has stronger absorption tendency. Fig. 6(c) represents the optical conductivity of the investigated compounds. The optical conductivity is a property of a material by which we can know how the material responds when it's exposed to light in terms of charge movement. It is totally revealed by how much it absorbs photons. This parameter can be calculated by the following formula:

$$\sigma(\omega) = n(\omega)\alpha(\omega)\,\frac{\omega}{2\pi} \tag{10}$$

The first peak of absorption $\sigma(\omega)$ value for $AlCuH_3$, $GaCuH_3$, and $InCuH_3$ are 1231.68 $\Omega^{-1}cm^{-1}$, 2828.59 $\Omega^{-1}cm^{-1}$, and 866.53 $\Omega^{-1}cm^{-1}$ at 0.48, 0.86, and 0.29 eV energy levels, respectively. For the studied materials, the greatest conductivity values are 8131.29 $\Omega^{-1}cm^{-1}$, 9914.13 $\Omega^{-1}cm^{-1}$, and 9143.49 $\Omega^{-1}cm^{-1}$ at the photon energy of 2.898, 3.77, and 3.796 eV, respectively. From $XCuH_3$, we have found that great optical conductivity across the 3–4.5 eV spectral region. The $GaCuH_3$ material has higher conductivity than $AlCuH_3$ and $InCuH_3$.

The electron loss function is a property of a material that occurs when energy dissipation occurs due to electrons moving rapidly or quickly, which is often referred to as plasmon losses. The loss function is often directly related to the scattering of incoming electrons. The peak of the loss function is related to the plasma frequency. We can calculate the loss function of a material using the following formula [90,91]:

$$L(\omega) = \frac{\varepsilon_2(\omega)}{\varepsilon_1^2(\omega) + \varepsilon_2^2(\omega)} \tag{11}$$

Fig. 6(d) plots the loss function $L(\omega)$ for $AlCuH_3$, $GaCuH_3$, and $InCuH_3$. From this, we can find the peak loss function in the UV region. The highest values of loss function are 0.70, 0.73, and 1.08 in the photon energy of 12 eV, these loss function values are particularly small that

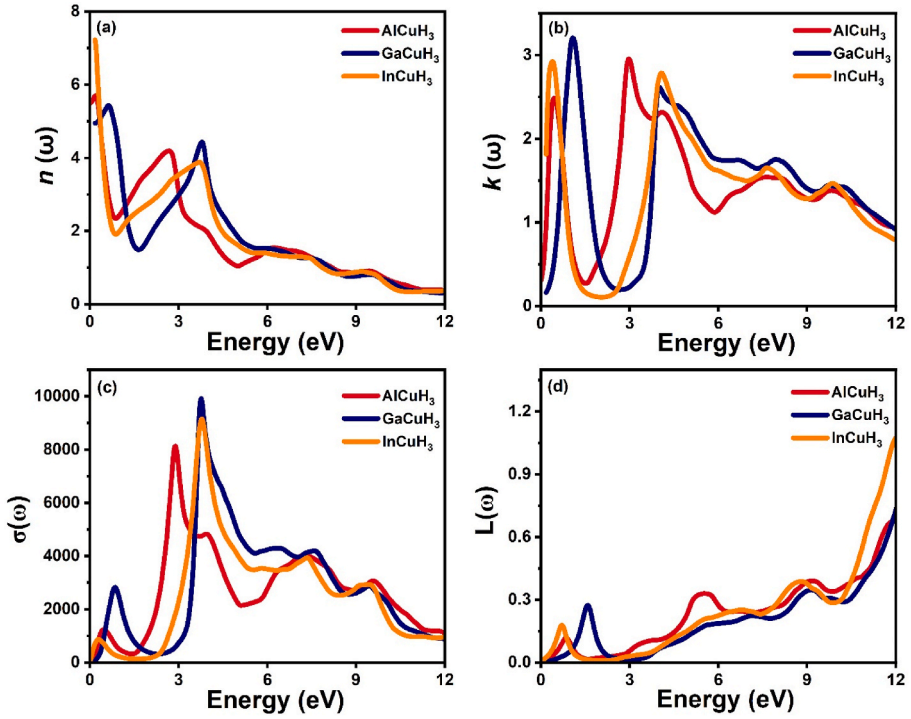

Fig. 6. (a) $n(\omega)$: Refractive index, **(b)** $k(\omega)$: Extinction coefficient, **(c)** $\sigma(\omega)$: Conductivity, and **(d)** $L(\omega)$: Loss function.

indicates we can use these materials in a hydrogen storage system.

3.5. Mechanical properties

Continuum mechanics is a valuable theory for understanding the physical response and intrinsic characteristics of solid matter. By Density functional theory (DFT), we can assess the accuracy of the result and conduct a comprehensive comparison between empirical and theoretical research. The elastic properties of a material can be calculated by this method [92]. In terms of continuum, considering the energy and stress methodology, the elastic constant can be calculated.

This approach employs a series of deformation tensors to modify the structure under the applied strain [93]. The strain iteration method determines elastic constants by analyzing the change in energy of a material when it is stretched or compressed, utilizing calculations from density functional theory (DFT). The material's mechanical behavior can be determined by the elastic constant, which is denoted by C_{ij} [93].

For hydrogen storage, a compound's mechanical stability is essential. To determine the mechanical stability, it needs to calculate the mechanical properties of the selected compound. For calculating the stability, the elastic constants, mainly C_{11}, C_{12}, and C_{44}, are critical parameters used in the Born-Huang criteria [94]. There are some conditions that needs to be satisfied for mechanical stability:

$C_{11} > 0, C_{44} > 0, (C_{11} - C_{12}) > 0, (C_{11} + 2C_{12}) > 0, C_{12} < B < C_{11}$

The data in Figs. 7 and 8 demonstrate the elastic coefficients and parameters for predicting the nature and mechanically stable compounds.

$$A = \frac{2C_{44}}{C_{11} - C_{12}} \tag{12}$$

$$B = \frac{C_{11} + 2C_{12}}{3} \tag{13}$$

$$G_v = \frac{C_{11} - C_{12} + 3C_{44}}{5} \tag{14}$$

$$G_R = \frac{5C_{44}(C_{11} - C_{12})}{4C_{44} + 3(C_{11} - C_{12})} \tag{15}$$

$$G = \frac{G_v + G_R}{2} \tag{16}$$

$$C_P = C_{12} - C_{44} \tag{17}$$

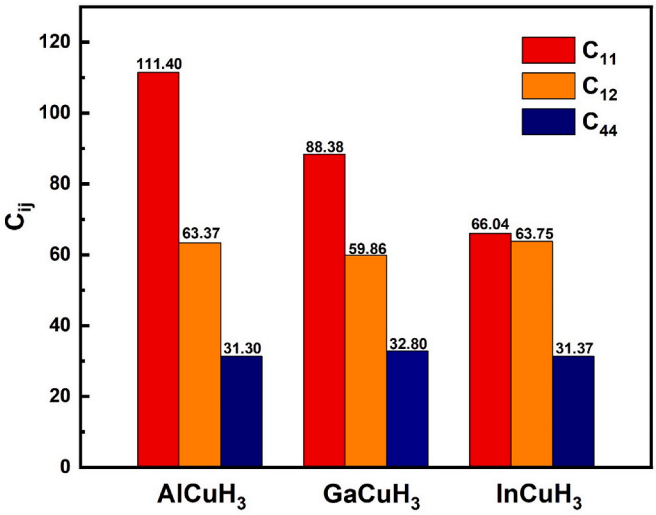

Fig. 7. Computed elastic constant (C_{ij}) of $AlCuH_3$, $GaCuH_3$, and $InCuH_3$.

The bulk modulus, denoted by B, is the mechanical characteristics that express a material resistance to compression. From investigated three materials, $AlCuH_3$ has the highest bulk modulus (79.38) followed by the $GaCuH_3$ (69.37), and $InCuH_3$ (64.52) which shown in Fig. 8(a). Hence, $AlCuH_3$ has better resistance to compression than $GaCuH_3$ and $InCuH_3$. The value of Shear modulus G is calculated by the values of $G_v$and G_R, is considered by the median of their average. This shear modulus value describes a material's stability to the shear forces, $AlCuH_3$ has the highest shear modulus (28.15) among $GaCuH_3$ (23.48) and $InCuH_3$ (10.99), shown in Fig. 8(b).

Young modulus is represented by E and it is defined by:

$$E = \frac{9BG}{3B + G} \tag{18}$$

Young modulus is a mechanical property that defines a material's hardness. By analyzing Fig. 8(c), it is clear that $AlCuH_3$ is harder than $GaCuH_3$ and $InCuH_3$. Because $AlCuH_3$ has a higher Young modulus (75.54) value than $GaCuH_3$ (63.30) and $InCuH_3$ (31.22).

To know whether a material has a covalent bond or an ionic bond, the Poisson ratio is used, and it is denoted by v. This Poisson is calculated by:

$$v = \frac{(3B - 2G)}{2(2B + G)} \tag{19}$$

If the Poisson ratio value is greater than 0.25, the material is generally considered to have ionic bonding [82] and also considered as ductile [95], and if this value is less than 0.25, then the material is considered to have covalent bonding and brittle. From Fig. 8(d), we observe that all three materials have a Poisson ratio greater than 0.25. Hence, this indicates that these materials exhibit ionic bonding and also display ductile characteristics. The Pugh ratio can be known by the ratio of B to G. A material is brittle or ductile, which can be known by the Pugh ratio. If the Pugh ratio is less than 1.75, the material exhibits brittle characteristics; if neither Pugh ratio is greater than 1.75, the material displays ductile characteristics. In Fig. 8(e), we investigated that all three materials show ductile characteristics as their Pugh ratio is less than 1.75.

The Cauchy pressure is another standard that can determine a material's brittleness or ductility. To find the Cauchy pressure, the value of C_{12} must be reduced by the value of C_{44}. For ductile characteristics, this value should be positive, and the value of $AlCuH_3$, $GaCuH_3$, and $InCuH_3$ is positive as shown in Fig. 8(f), and this value provides support for the conclusion that all three materials have ductile characteristics. The ductile nature and mechanical stability indicate the material's ability to withstand the internal stresses and volumetric changes during hydrogen cycling without fracturing, a critical property for long-term durability in a storage system.

If the anisotropic factor of a material equals 1, it is classified as isotropic; otherwise, it is considered anisotropic [96,97]. From Table 3, we observe that the three investigated materials do not equal 1; therefore, they exhibit anisotropic characteristics. There are relations between the average velocity of the wave and the Debye temperature, which means we need an effective wave velocity for the Debye temperature. By using these values, we can obtain average information about the states of the material, specifically its inter-atomic bonding state. Stronger interatomic bonding may be inferred from a higher average wave velocity and Debye temperature; it is evident that the interatomic bonding decreases.

3.6. Hydrogen storage

Metal hydrides have become an emerging material for hydrogen storage applications these days. However, to store hydrogen, there exists a requirement for sufficient gravimetric ability of matter; this is absent of high gravimetric capacity, which is the initial cause that limits the all-new use of hydrogen as a fuel. For using hydrogen as fuel, we need to

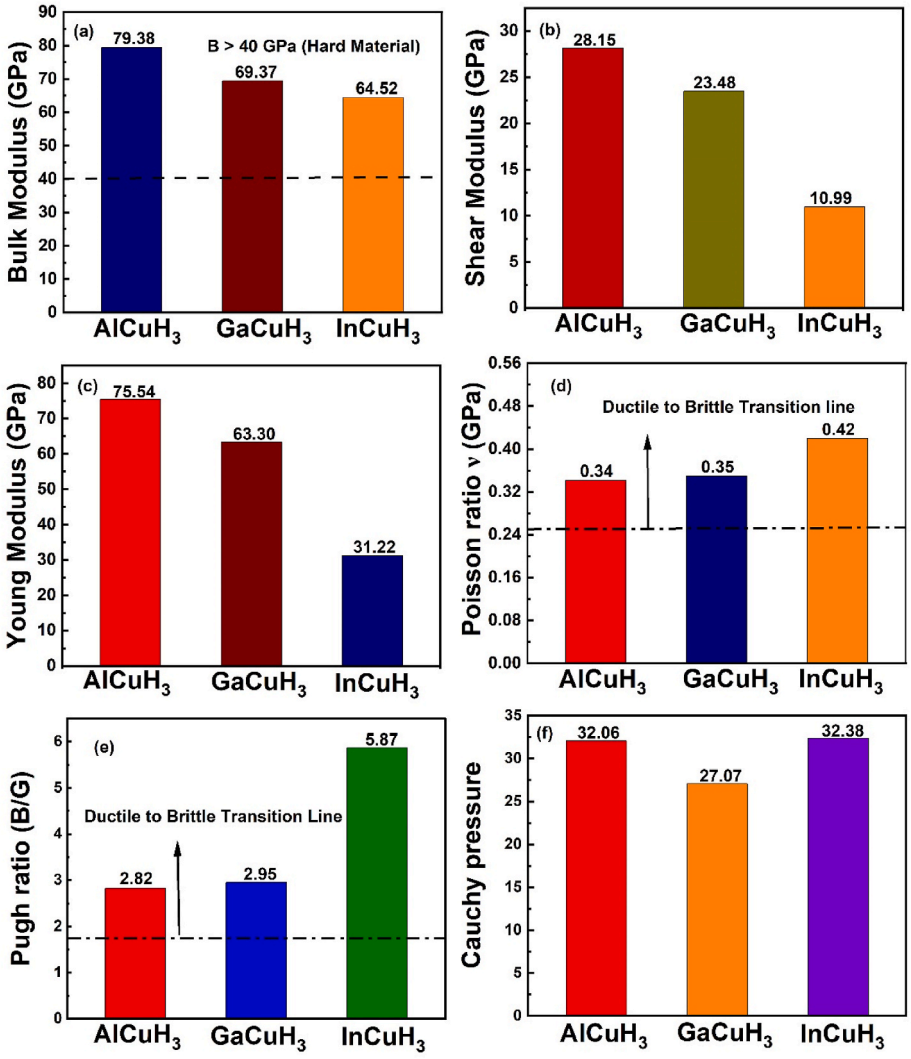

Fig. 8. Elastic Parameters of **(a)** Bulk Modulus, **(b)** Shear Modulus, **(c)** Young Modulus, **(d)** Poisson Ratio, **(e)** Pugh Ratio, and **(f)** Cauchy Pressure obtained for $XCuH_3$.

Table 3
Calculated elastic parameters of $XCuH_3$ (X = Al, Ga, In).

Parameters	$AlCuH_3$	$GaCuH_3$	$InCuH_3$
Anisotropy factor A	1.30	2.30	27.40
Voigt Modulus (Voigt) G_v	28.391	25.382	19.279
Reuss Modulus (Reuss) G_R	27.918	21.58	2.713
Average wave velocity V_m (m s^{-1})	3130.022	2433.912	1537.190
Debye temperature θ_D (K)	455.328	347.863	212.082

solve this so that our materials can store hydrogen molecules at a higher volume. There are various systems, like gas state storage, liquid state storage or solid-state storage technology. Scientists have been finding different kinds of materials, including metal hydride perovskites, to overcome this barrier of low gravimetric capacity. The gravimetric hydrogen storage capacity is the most reliable metric in approaching the maximal hydrogen storage capacity of a material; however, the actual gravimetric hydrogen storage capacity can be obtained via the following equation [80,98]:

$$C_{g_{wt}}\% = \left(\frac{\left(\frac{H}{M}\right) m_H}{\left(\frac{H}{M}\right) m_H + m_{Host}} \right) \times 100 \quad (20)$$

Where H/M is the atomic ratio of hydrogen to material, m_H is the molar mass of hydrogen, and m_{Host} is the molar mass of the material. From this equation, we find the gravimetric capacity of $AlCuH_3$, $GaCuH_3$, and $InCuH_3$ and the values are 3.23 %, 2.22 %, and 1.67 %, respectively. To be familiar with the hydrogen storage characteristics of our practiced structure and their applications in hydrogen storage use, we have also computed the desorption temperature (T_d) further. In terms of terminology, the desorption temperature refers to the temperature at which the hydrogen leaves the material; this is a critical parameter for evaluating the efficiency and practicality of storage materials in energy applications. The following reaction is used for the calculating Enthalpy of reactions

$$X + Cu + \frac{3}{2} H_2 \rightarrow XCuH_3 \quad (20)$$

For calculating desorption temperature, we use the following expression [99,100]:

$$\Delta G = \Delta H - T_d \Delta S \quad (21)$$

Considering $\Delta G = 0$, under normal conditions (Temperature, Pressure), then we get

$$T_d = \frac{-\Delta H}{\Delta S} \quad (22)$$

Where, ΔH is the calculated formation enthalpy, the entropy change of hydrogen is denoted by ΔS, the value of entropy change of hydrogen is −130.7 J/mol · K [103]. The hydrogen desorption temperatures for $AlCuH_3$, $GaCuH_3$, and $InCuH_3$ are 800.24 K, 829.88 K, and 868.40 K, respectively. These values are physically reasonable and align well with the desorption temperatures reported for other ternary hydrides with similar structures, such as $LiRhH_3$ (804.71K), $CsPtH_3$ (826.8K), $FrPtH_3$ (923.5K), $BeSnH_3$ (842.9K) [104–106]. If the desorption temperature is lower, it means this material releases hydrogen easily, and if the desorption temperature is higher, it means this material releases hydrogen with more thermal energy. Table 4 shows hydrogen capacity level of different hydride metal compounds compared with the present results of $AlCuH_3$, $GaCuH_3$ and $InCuH_3$ and reported data from the literature. The data set emphasizes the compositional effect on the hydrogen holding capacity for various perovskite-type hydrides. Therefore, all three materials can be suitable for hydrogen storage application but practical application is currently hindered by low gravimetric capacity and prohibitively high desorption temperatures, both consequences of excessive thermodynamic stability. Although these properties may be less attractive for mobile hydrogen applications, they could be suitable for stationary hydrogen storage, high operational temperature could be managed using waste industrial heat or concentrated solar thermal energy.

4. Conclusion

We analyze three perovskite type hydrides $AlCuH_3$, $GaCuH_3$, and $InCuH_3$, for hydrogen storage and also analyze their structural, mechanical, electronic, and optical properties in detail, by using the Wien2k code for accuracy and efficiency. For our investigated three materials, we found their optimized lattice parameter of 3.50 Å, 3.56 Å, and 3.69 Å, respectively. From the calculated value of tolerance factor and octahedral factor, we had known that these materials are structurally stable. The thermo-dynamical stability is confirmed by the negative value of formation energy for all three materials. By Born-Huang stability criteria, the mechanical stability is evaluated; from this analysis, it is visible that all these materials are ductile. We had previously examined these three metals, where band structure indicated metallic behavior with zero band gaps. The anisotropic nature of these three materials can be realized from anisotropic factor. Lastly, we found the gravimetric hydrogen storage capacity for $AlCuH_3$, $GaCuH_3$, and $InCuH_3$ are 3.23 %, 2.22 % and 1.67 %, respectively. From the overall analysis of these three materials, we can say all three materials can be useful for stationary hydrogen storage capacity is significantly strengthen. Future work will investigate elemental doping to destabilize the hydride phase and reduce the decomposition temperature, and nano-structuring to facilitate kinetics and possibly increase capacity.

CRediT authorship contribution statement

R.M. Tanvir: Writing – original draft, Validation, Methodology, Formal analysis, Data curation. **S. Tanvir:** Writing – original draft, Validation, Investigation. **Md Al-Amin:** Writing – review & editing, Validation, Investigation. **A. Rayhan:** Writing – review & editing, Validation. **S. Mahmud:** Writing – review & editing, Validation, Supervision, Project administration, Methodology, Formal analysis, Conceptualization.

Declaration of competing interest

The authors declare that they have no known competing financial interests or personal relationships that could have appeared to influence the work reported in this paper.

Table 4
Hydrogen capacity of some hydride compounds from literature and present work (Cwt%).

Compounds	C_{wt} %	Ref.
$AlCuH_3$	3.23	Present Study
$GaCuH_3$	2.22	Present Study
$InCuH_3$	1.67	Present Study
$CaCuH_3$	2.85	[48]
$SrCuH_3$	1.97	[48]
$CsBH_3$	2.19	[101]
$RbBH_3$	3.09	[101]
$CoCuH_3$	2.28	[39]
$NiCuH_3$	3.0	[39]
$ZnCuH_3$	2.7	[39]
$RbGaH_3$	2.5	[38]
$CsGaH_3$	2.0	[38]
$FrGaH_3$	2.1	[38]
$KCuH_3$	2.78	[102]
$RbCuH_3$	1.95	[102]

Data availability

Data will be made available on request.

References

[1] M. Höök, X. Tang, Depletion of fossil fuels and anthropogenic climate change—A review, Energy Policy 52 (Jan. 2013) 797–809, https://doi.org/10.1016/J.ENPOL.2012.10.046.

[2] M. Ganjian, et al., ZnS shell-like CdS quantum dot-sensitized solar cell grown by SILAR approach; effect of electrolyte, counter electrode, and shell thickness, Vacuum 146 (Dec. 2017) 548–553, https://doi.org/10.1016/J.VACUUM.2017.02.007.

[3] H. Lei, et al., Converting H_2O and CO_2 into chemical fuels by nickel via friction, Surf. Interfaces 46 (Mar. 2024) 104203, https://doi.org/10.1016/J.SURFIN.2024.104203.

[4] M.B. Bahari, A.A. Jalil, C.R. Mamat, N.S. Hassan, H.D. Setiabudi, D.V.N. Vo, Insight into the development of silica-based materials as photocatalysts for CO_2 photoconversion towards CH_3OH: a review and recent progress, Surf. Interfaces 31 (Jul. 2022) 102049, https://doi.org/10.1016/J.SURFIN.2022.102049.

[5] F. Perera, Pollution from fossil-fuel combustion is the leading environmental threat to global pediatric health and equity: solutions exist, Int. J. Environ. Res. Publ. Health 15 (1) (Dec. 2017) 16, https://doi.org/10.3390/IJERPH15010016, 2018, Vol. 15, Page 16.

[6] N. Armaroli, V. Balzani, The legacy of fossil fuels, Chem. Asian J. 6 (3) (Mar. 2011) 768–784, https://doi.org/10.1002/ASIA.201000797.

[7] M. Zaman, et al., Revealing hydrogen storage, thermodynamic, electronic, and mechanical aspects of perovskite hydrides $GaXH_3$ (X = Si, Ge): First-principles approach, Energy 337 (Nov. 2025) 138578, https://doi.org/10.1016/J.ENERGY.2025.138578.

[8] F. Johnsson, J. Kjärstad, J. Rootzén, The threat to climate change mitigation posed by the abundance of fossil fuels, Clim. Policy 19 (2) (Feb. 2019) 258–274, https://doi.org/10.1080/14693062.2018.1483885.

[9] S. Al, Theoretical investigations of elastic and thermodynamic properties of $LiXH_4$ compounds for hydrogen storage, Int. J. Hydrogen Energy 44 (3) (Jan. 2019) 1727–1734, https://doi.org/10.1016/J.IJHYDENE.2018.11.156.

[10] S.M. Jokar, et al., The recent areas of applicability of palladium based membrane technologies for hydrogen production from methane and natural gas: a review, Int. J. Hydrogen Energy 48 (16) (Feb. 2023) 6451–6476, https://doi.org/10.1016/J.IJHYDENE.2022.05.296.

[11] A. Ayyaz, et al., Predicting hydrogen storage, mechanical, thermodynamic, and electronic characteristics of perovskite hydrides $NaBH_3$ (B = Cu, Zn, Cd): a first-principles study, Int. J. Hydrogen Energy 163 (Sep. 2025) 150780, https://doi.org/10.1016/J.IJHYDENE.2025.150780.

[12] M.A. Aminudin, S.K. Kamarudin, B.H. Lim, E.H. Majilan, M.S. Masdar, N. Shaari, An overview: current progress on hydrogen fuel cell vehicles, Int. J. Hydrogen Energy 48 (11) (Feb. 2023) 4371–4388, https://doi.org/10.1016/J.IJHYDENE.2022.10.156.

[13] Y. Kang, et al., Study on the hydrogen leakage diffusion behavior by obstacles in confined spaces, Fuel 358 (Feb. 2024) 130110, https://doi.org/10.1016/J.FUEL.2023.130110.

[14] M. Genovese, D. Blekhman, P. Fragiacomo, An exploration of safety measures in hydrogen refueling stations: delving into hydrogen equipment and technical performance, Hydrogen 5 (1) (Feb. 2024) 102–122, https://doi.org/10.3390/HYDROGEN5010007, 2024, Vol. 5, Pages 102-122.

[15] E. Kalihonda, E. Igbineweka, S. Chowdhury, Integrating hydrogen as an energy storage for renewable energy systems: a comprehensive review. Proceedings of the 32nd Southern African Universities Power Engineering Conference, SAUPEC 2024, 2024, https://doi.org/10.1109/SAUPEC60914.2024.10445099.

[16] S. Bosu, N. Rajamohan, Recent advancements in hydrogen storage - comparative review on methods, operating conditions and challenges, Int. J. Hydrogen Energy 52 (Jan. 2024) 352–370, https://doi.org/10.1016/J.IJHYDENE.2023.01.344.

[17] X. Yan, W. Zheng, Y. Wei, Z. Yan, Current status and economic analysis of green hydrogen energy industry chain, Processes 12 (2) (Feb. 2024) 315, https://doi.org/10.3390/PR12020315, 2024, Vol. 12, Page 315.

[18] J. Ye, et al., Optimization design of solid-state hydrogen storage device for fuel cell forklift, J. Alloys Compd. 970 (Jan. 2024) 172242, https://doi.org/10.1016/J.JALLCOM.2023.172242.

[19] C. Drawer, J. Lange, M. Kaltschmitt, Metal hydrides for hydrogen storage – identification and evaluation of stationary and transportation applications, J. Energy Storage 77 (Jan. 2024) 109988, https://doi.org/10.1016/J.EST.2023.109988.

[20] O. Utomo, M. Abeysekera, C.E. Ugalde-Loo, Optimal operation of a hydrogen storage and fuel cell coupled integrated energy System, Sustainability 13 (6) (Mar. 2021) 3525, https://doi.org/10.3390/SU13063525, 2021, Vol. 13, Page 3525.

[21] S. Zerroug, F. Ali Sahraoui, N. Bouarissa, Elastic properties of $Al_xIn_{1-x}P_ySb_{1-y}$ and $Al_xGa_{1-x}P_ySb_{1-y}$ lattice matched to InAs substrate, Mater. Lett. 60 (4) (Feb. 2006) 546–550, https://doi.org/10.1016/J.MATLET.2005.09.032.

[22] S. Mnasri, S. Abdi-Ben Nasrallah, N. Sfina, N. Bouarissa, M. Said, Electronic, lattice vibration and mechanical properties of CdTe, ZnTe, MnTe, MgTe, HgTe and their ternary alloys, Semicond. Sci. Technol. 24 (9) (Jul. 2009) 095008, https://doi.org/10.1088/0268-1242/24/9/095008.

[23] N. Bouarissa, Electronic properties of $Ga_xIn_{1-x}P$ from pseudopotential calculations, Mater. Chem. Phys. 124 (1) (Nov. 2010) 336–341, https://doi.org/10.1016/J.MATCHEMPHYS.2010.06.043.

[24] S. Ferahtia, S. Saib, N. Bouarissa, S. Benyettou, Structural parameters, elastic properties and piezoelectric constants of wurtzite ZnS and ZnSe under pressure, Superlattice. Microst. 67 (Mar. 2014) 88–96, https://doi.org/10.1016/J.SPMI.2013.12.021.

[25] A. Ayyaz, et al., DFT investigation of thermodynamic, electronic, optical, and mechanical properties of $XLiH_3$ (X= Mg, Ca, Sr, and Ba) hydrides for hydrogen storage and energy harvesting, Mater. Sci. Semicond. Process. 186 (Feb. 2025) 109020, https://doi.org/10.1016/J.MSSP.2024.109020.

[26] M. Baricco, et al., Hydrogen storage and handling with hydrides, Pure Appl. Chem. 96 (4) (Apr. 2024) 511–524, https://doi.org/10.1515/PAC-2023-1134/ASSET/GRAPHIC/J_PAC-2023-1134_FIG_005.JPG.

[27] Y. Li, et al., MOFs-Based materials for solid-state hydrogen storage: strategies and perspectives, Chem. Eng. J. 485 (Apr. 2024) 149665, https://doi.org/10.1016/J.CEJ.2024.149665.

[28] S. Wang, et al., Preparation and properties of hydrogen storage materials of porous carbon composite diatom skeleton, Int. J. Hydrogen Energy 64 (Apr. 2024) 773–780, https://doi.org/10.1016/J.IJHYDENE.2024.03.361.

[29] T. Manda, et al., A data-guided approach for the evaluation of zeolites for hydrogen storage with the aid of molecular simulations, J. Mol. Model. 30 (2) (Feb. 2024) 1–14, https://doi.org/10.1007/S00894-024-05837-Z/METRICS.

[30] A. Irham, M.F. Roslan, K.P. Jern, M.A. Hannan, T.M.I. Mahlia, Hydrogen energy storage integrated grid: a bibliometric analysis for sustainable energy production, Int. J. Hydrogen Energy 63 (Apr. 2024) 1044–1087, https://doi.org/10.1016/J.IJHYDENE.2024.03.235.

[31] L. Zhang, et al., A comprehensive review of the promising clean energy carrier: hydrogen production, transportation, storage, and utilization (HPTSU) technologies, Fuel 355 (Jan. 2024) 129455, https://doi.org/10.1016/J.FUEL.2023.129455.

[32] J. Rani, J. Kumari, S.K. Chand, S. Chand, Climate Change and Renewable Energy (2024) 153–171, https://doi.org/10.1007/978-981-97-1685-2_9.

[33] W. Azeem, M.K. Shahzad, Y.H. Wong, M.B. Tahir, Ab-initio calculations for the study of the hydrogen storage properties of $CsXH_3$ (X= Co, Zn) perovskite-type hydrides, Int. J. Hydrogen Energy 50 (Jan. 2024) 305–313, https://doi.org/10.1016/J.IJHYDENE.2023.07.072.

[34] Y. Bouhadda, M. Bououdina, N. Fenineche, Y. Boudouma, Elastic properties of perovskite-type hydride $NaMgH_3$ for hydrogen storage, Int. J. Hydrogen Energy 38 (3) (Feb. 2013) 1484–1489, https://doi.org/10.1016/J.IJHYDENE.2012.11.047.

[35] B. Rehmat, M.A. Rafiq, Y. Javed, Z. Irshad, N. Ahmed, S.M. Mirza, Elastic properties of perovskite-type hydrides $LiBeH_3$ and $NaBeH_3$ for hydrogen storage, Int. J. Hydrogen Energy 42 (15) (Apr. 2017) 10038–10046, https://doi.org/10.1016/J.IJHYDENE.2017.01.109.

[36] A. Ayyaz, et al., First principles study of hydrogen storage, electronic, thermodynamic, and mechanical aspects of Perovskite hydrides $LiBH_3$ (B = Cu, Zn, Cd), J. Power Sources 654 (Oct. 2025) 237803, https://doi.org/10.1016/J.JPOWSOUR.2025.237803.

[37] K. Ikeda, T. Sato, S.I. Orimo, Perovskite-type hydrides - synthesis, structures and properties, Int. J. Mater. Res. 99 (5) (May 2008) 471–479, https://doi.org/10.3139/146.101671/MACHINEREADABLECITATION/RIS.

[38] R.M.A. Khalil, S. Hayat, M.I. Hussain, A.M. Rana, F. Hussain, DFT based first principles study of novel combinations of perovskite-type hydrides $XGaH_3$(X = Rb, Cs, Fr) for hydrogen storage applications, AIP Adv. 11 (2) (Feb. 2021), https://doi.org/10.1063/5.0037790/964024.

[39] S. Hayat, R.M.A. Khalil, M.I. Hussain, A.M. Rana, F. Hussain, First-principles investigations of the structural, optoelectronic, magnetic and thermodynamic properties of hydride perovskites $XCuH_3$ (X = Co, Ni, Zn) for hydrogen storage applications, Optik 228 (Feb. 2021) 166187, https://doi.org/10.1016/J.IJLEO.2020.166187.

[40] G. Surucu, A. Candan, A. Gencer, M. Isik, First-principle investigation for the hydrogen storage properties of $NaXH_3$ (X= Mn, Fe, Co) perovskite type hydrides, Int. J. Hydrogen Energy 44 (57) (Nov. 2019) 30218–30225, https://doi.org/10.1016/J.IJHYDENE.2019.09.201.

[41] P. Khajondetchairit, M. Rittiruam, T. Saelee, P. Hirunsit, S. Praserthdam, S. Suthirakun, A DFT study on how vanadium affects hydrogen storage kinetics in magnesium nickel hydride, Int. J. Hydrogen Energy 48 (53) (Jun. 2023) 20378–20387, https://doi.org/10.1016/J.IJHYDENE.2023.02.080.

[42] K.S. Nivedhitha, et al., Advances in hydrogen storage with metal hydrides: mechanisms, materials, and challenges, Int. J. Hydrogen Energy 61 (Apr. 2024) 1259–1273, https://doi.org/10.1016/J.IJHYDENE.2024.02.335.

[43] N.A.A. Rusman, M. Dahari, A review on the current progress of metal hydrides material for solid-state hydrogen storage applications, Int. J. Hydrogen Energy 41 (28) (Jul. 2016) 12108–12126, https://doi.org/10.1016/J.IJHYDENE.2016.05.244.

[44] W. Khan, The first principles insights of aluminum-based hydrides for hydrogen storage application, Int. J. Hydrogen Energy 63 (Apr. 2024) 596–608, https://doi.org/10.1016/J.IJHYDENE.2024.03.180.

[45] M. Rkhis, et al., Recent advances in magnesium hydride for solid-state hydrogen storage by mechanical treatment: a DFT study, Int. J. Hydrogen Energy 48 (91) (Nov. 2023) 35650–35660, https://doi.org/10.1016/J.IJHYDENE.2023.05.267.

[46] J. Sun, First-Principles calculations of novel materials [Online]. Available: https://repository.lib.fsu.edu/islandora/object/fsu%3A253146/, 2015. (Accessed 12 August 2025).

[47] L. Ruihan, H. Feng, X. Ting, L. Yongzhi, Z. Xin, Z. Jiaqi, Progress in the application of first principles to hydrogen storage materials, Int. J. Hydrogen Energy 56 (Feb. 2024) 1079–1091, https://doi.org/10.1016/J.IJHYDENE.2023.12.259.

[48] B. Ahmed, M.B. Tahir, A. Ali, M. Sagir, First-principles screening of structural, electronic, optical and elastic properties of Cu-based hydrides-perovskites $XCuH_3$ (X=Ca and Sr) for hydrogen storage applications, Int. J. Hydrogen Energy 54 (Feb. 2024) 1001–1007, https://doi.org/10.1016/J.IJHYDENE.2023.11.239.

[49] J. Hafner, Ab-initio simulations of materials using VASP: Density-functional theory and beyond, J. Comput. Chem. 29 (13) (Oct. 2008) 2044–2078, https://doi.org/10.1002/JCC.21057.

[50] F. Tran, P. Blaha, Accurate band gaps of semiconductors and insulators with a semilocal exchange-correlation potential, Phys. Rev. Lett. 102 (22) (Jun. 2009) 226401, https://doi.org/10.1103/PHYSREVLETT.102.226401/FIGURES/2/THUMBNAIL.

[51] M.A. Ullah, K.N. Riaz, M. Rizwan, Computational evaluation of $KMgO_3$-xHx as an efficient hydrogen storage material, J. Energy Storage 70 (Oct. 2023) 108030, https://doi.org/10.1016/J.EST.2023.108030.

[52] W. Travis, E.N.K. Glover, H. Bronstein, D.O. Scanlon, R.G. Palgrave, On the application of the tolerance factor to inorganic and hybrid halide perovskites: a revised system, Chem. Sci. 7 (7) (Jun. 2016) 4548–4556, https://doi.org/10.1039/C5SC04845A.

[53] N. Xu, et al., First-principles investigations for the hydrogen storage properties of XVH_3 (X=Na, K, Rb, Cs) perovskite type hydrides, J. Mater. Res. Technol. 26 (Sep. 2023) 4825–4834, https://doi.org/10.1016/J.JMRT.2023.08.218.

[54] M.I. Hussain, R.M.A. Khalil, Density functional theory studies of the structural, optoelectronic, bond stiffness and lattice dynamical properties of double perovskite oxides M_2YVO_6 (M= Mg, Sr): promising candidates for optoelectronic applications, Mater. Sci. Semicond. Process. 152 (Dec. 2022) 107050, https://doi.org/10.1016/J.MSSP.2022.107050.

[55] M.I. Hussain, R.M.A. Khalil, F. Hussain, Computational exploration of structural, electronic, and optical properties of novel combinations of inorganic ruddlesden–popper layered perovskites Bi_2XO_4 (X = Be, mg) using tran and blaha-modified Becke–Johnson approach for optoelectronic applications, Energy Technol. 9 (5) (May 2021) 2001026, https://doi.org/10.1002/ENTE.202001026.

[56] M.I. Hussain, R.M.A. Khalil, F. Hussain, A.M. Rana, DFT-based insight into the magnetic and thermoelectric characteristics of $XTaO_3$ (X = Rb, Fr) ternary perovskite oxides for optoelectronic applications, Int. J. Energy Res. 45 (2) (Feb. 2021) 2753–2765, https://doi.org/10.1002/ER.5968.

[57] M.I. Hussain, R.M. Arif Khalil, F. Hussain, A.M. Rana, G. Murtaza, M. Imran, Probing the structural, electronic, mechanical strength and optical properties of tantalum-based oxide perovskites $ATaO_3$ (A = Rb, Fr) for optoelectronic applications: First-principles investigations, Optik 219 (Oct. 2020) 165027, https://doi.org/10.1016/J.IJLEO.2020.165027.

[58] F.N. Li, et al., Investigations of structural, electronic and optical properties of TM-GaO_3 (TM = Sc, Ti, Ag) perovskite oxides for optoelectronic applications: a first principles study, Mater. Res. Express 7 (1) (Jan. 2020) 015906, https://doi.org/10.1088/2053-1591/AB619C.

[59] M. Ahmed, R. Fatima, A. Bakar, A. Orynbassar, N. Shynarbek, Y. Khairy, Exploration of hydrides $XSrH_3$(X=Cs,Fr) for hydrogen storage applications: a first principles study, Int. J. Hydrogen Energy 83 (Sep. 2024) 460–471, https://doi.org/10.1016/J.IJHYDENE.2024.08.076.

[60] A. Bakar, et al., Computational investigations of MnNiCuSb alloy for structural, elasto-mechanical and vibrational properties, Modern Phys. Lett. 33 (23) (Aug. 2019), https://doi.org/10.1142/S0217984919502762, 10.1142/S0217984919502762.

[61] M. Ahmed, A. Afaq, A. Bakar, M. Asif, in: Density functional study of CoFeCrZ (Z=Al, Si, Ga, Ge) quaternary Heusler alloys for phonon spectra, 34, Sep. 2020, https://doi.org/10.1142/S021797922050215X, 10.1142/S021797922050215X, 25.

[62] A. Afaq, H. Maaz, A. Bakar, M.I. Jamil, Reststrahlen band studies of RuCrX (X = Si, Ge, sn) half heusler alloys, J. Electron. Mater. 48 (8) (Aug. 2019) 5323–5327, https://doi.org/10.1007/S11664-019-07342-Z/METRICS.

[63] A. Afaq, A. Bakar, N. Khan, A. Asif, in: Reststrahlen band studies in cubic perovskite materials $SmXO_3$ (X = Al, Co) by computational investigations, 34, Aug. 2020, https://doi.org/10.1142/S0217979220502069, 10.1142/S0217979220502069, 21.

[64] N. Arikan, H.Y. Ocak, G. Dikici Yıldız, Y.G. Yıldız, R. Ünal, Investigation of the mechanical, electronic and phonon properties of X_2ScAl (X = Ir, Os, and Pt) Heusler compounds, J. Kor. Phys. Soc. 76 (10) (May 2020) 916–922, https://doi.org/10.3938/JKPS.76.916/METRICS.

[65] S. Al, N. Cavdar, N. Arikan, Computational evaluation of comprehensive properties of MgX3H8 (X = Sc, Ti and Zr) as effective solid state hydrogen storage materials, J. Energy Storage 80 (Mar. 2024) 110402, https://doi.org/10.1016/J.EST.2023.110402.

[66] A. Ayyaz, et al., Exploring hydrogen storage potential, thermodynamic, and optoelectronic characteristics of novel double perovskite hydrides Na_2LiXH_6 (X = Al, Sc, and Ga): DFT analysis, J. Energy Storage 122 (Jun. 2025) 116650, https://doi.org/10.1016/J.EST.2025.116650.

[67] A. Boulahouache, M. Benlembarek, N. Salhi, A.M. Djaballah, C. Rabia, M. Trari, Preparation, characterization and electronic properties of $LaFeO_3$ perovskite as photocatalyst for hydrogen production, Int. J. Hydrogen Energy 48 (39) (May 2023) 14650–14658, https://doi.org/10.1016/J.IJHYDENE.2022.12.327.

[68] Y. Zhu, Y. Liang, Y. Pu, J. Xiong, Investigation for the hydrogen storage properties of $XCrH_3$ (X=Na, K) and KYH_3(Y= Mo, W) perovskite type hydrides based on first-principles, Int. J. Hydrogen Energy 71 (Jun. 2024) 239–249, https://doi.org/10.1016/J.IJHYDENE.2024.05.292.

[69] M. Usman, J. ur Rehman, M.B. Tahir, A. Hussain, Structural, electronics, magnetic, optical, mechanical and hydrogen storage properties of Ga-based hydride-perovskites $XGaH_3$ (X = K, Li), Int. J. Energy Res. 46 (11) (Sep. 2022) 15617–15626, https://doi.org/10.1002/ER.8257.

[70] S. Benlamari, et al., Structural, electronic, elastic, and thermal properties of $CaNiH_3$ perovskite obtained from first-principles calculations, Chin. Phys. B 27 (3) (Mar. 2018) 037104, https://doi.org/10.1088/1674-1056/27/3/037104.

[71] G. Surucu, A. Gencer, A. Candan, H.H. Gullu, M. Isik, $CaXH_3$ (X = Mn, Fe, Co) perovskite-type hydrides for hydrogen storage applications, Int. J. Energy Res. 44 (3) (Mar. 2020) 2345–2354, https://doi.org/10.1002/ER.5062.

[72] H. Shabbir, M. Usman, J.U. Rehman, D. Pan, S.M. Ali, R. Alotaibi, A DFT investigation of Sc-based perovskite-type hydrides $XScH_3$ (X = K, Na) for hydrogen storage application, J. Comput. Electron. 23 (6) (Dec. 2024) 1238–1248, https://doi.org/10.1007/S10825-024-02217-X/METRICS.

[73] Z. ur Rehman, et al., A DFT study of structural, electronic, mechanical, phonon, thermodynamic, and H2 storage properties of lead-free perovskite hydride $MgXH_3$(X=Cr, Fe, Mn), J. Phys. Chem. Solid. 186 (Mar. 2024) 111801, https://doi.org/10.1016/J.JPCS.2023.111801.

[74] M.M. Parvaiz, A. Khalil, M. Bilal Tahir, S. Ayub, T.E. Ali, H.T. Masood, A DFT investigation on structural, electronic, magnetic, optical, elastic and hydrogen storage properties of Ru-based hydride-perovskites $XRuH_3$ (X = Cr, V, Ni), RSC Adv. 14 (12) (Mar. 2024) 8385–8396, https://doi.org/10.1039/D4RA00204K.

[75] A. Mera, M.A. Rehman, First-principles investigation for the hydrogen storage properties of $AeSiH_3$ (Ae = Li, K, Na, Mg) perovskite-type hydrides, Int. J. Hydrogen Energy 50 (Jan. 2024) 1435–1447, https://doi.org/10.1016/J.IJHYDENE.2023.09.286.

[76] Z. ur Rehman, et al., Ab initio insight into the physical properties of $MgXH_3$ (X = Co, Cu, Ni) lead-free perovskite for hydrogen storage application, Environ. Sci. Pollut. Control Ser. 30 (53) (Nov. 2023) 113889–113902, https://doi.org/10.1007/S11356-023-30279-0/METRICS.

[77] A. Ayyaz, et al., Investigation of hydrogen storage and energy harvesting potential of double perovskite hydrides A_2LiCuH_6 (A = Be/Mg/Ca/Sr): a DFT approach, Int. J. Hydrogen Energy 102 (Feb. 2025) 1329–1339, https://doi.org/10.1016/J.IJHYDENE.2025.01.117.

[78] W. Zhang, J. Guo, X. Lv, F. Zhang, Combined machine learning and high-throughput calculations predict heyd-scuseria-ernzerhof band gap of 2D materials and potential MoSi2N4 heterostructures, J. Phys. Chem. Lett. 15 (20) (May 2024) 5413–5419, https://doi.org/10.1021/ACS.JPCLETT.4C01013/SUPPL_FILE/JZ4C01013_SI_007.PDF.

[79] A. Ayyaz, et al., Structural, morphological, elastic, optoelectronic and thermoelectric properties of lead-free double perovskite $Na_2AgBiBr_6$ for photovoltaic applications: experimental and DFT insight, Ceram. Int. 50 (9) (May 2024) 15261–15272, https://doi.org/10.1016/J.CERAMINT.2024.02.002.

[80] M. Usman, J. ur Rehman, M.B. Tahir, A. Hussain, Structural, electronics, magnetic, optical, mechanical and hydrogen storage properties of Ga-based hydride-perovskites $XGaH_3$ (X = K, Li), Int. J. Energy Res. 46 (11) (Sep. 2022) 15617–15626, https://doi.org/10.1002/ER.8257.

[81] A. Ayyaz, et al., DFT-based comparative study of mechanical, electro-optic, and transport response of halide double perovskites Na_2MAlZ_6 (M = Ag, Cu; Z = Br, I) for green energy applications, Mater. Sci. Eng., B 317 (Jul. 2025) 118250, https://doi.org/10.1016/J.MSEB.2025.118250.

[82] M. Usman, et al., A computational insight of $LiTH_3$ (T = Y, Zr) perovskite-type hydrides for hydrogen storage application, Int. J. Hydrogen Energy 110 (Mar. 2024) 764–772, https://doi.org/10.1016/J.IJHYDENE.2025.02.210.

[83] R.M.A. Khalil, S. Hayat, M.I. Hussain, A.M. Rana, F. Hussain, DFT based first principles study of novel combinations of perovskite-type hydrides $XGaH_3$(X = Rb, Cs, Fr) for hydrogen storage applications, AIP Adv. 11 (2) (Feb. 2021), https://doi.org/10.1063/5.0037790/964024.

[84] A. Ayyaz, et al., DFT aided comparative screening of mechanical, optoelectronic, and transport properties of double perovskites Cs_2ScAuX_6 (X = Cl, Br, and I) for green energy applications, Inorg. Chem. Commun. 165 (Jul. 2024) 112527, https://doi.org/10.1016/J.INOCHE.2024.112527.

[85] S. Mahmud, M.A.U.Z. Atik, M.N. Mostakim, M. Tarekuzzaman, M.Z. Hasan, Investigation of direct small bandgap Cs_2AuInX_6 (X = F/Cl) double perovskites for energy harvesting technology employing DFT, Comput. Conden. Matter 40 (Sep. 2024) e00950, https://doi.org/10.1016/J.COCOM.2024.E00950.

[86] A. Ayyaz, S. Saidi, N. Dawas Alkhaldi, G. Murtaza, N. Sfina, Q. Mahmood, Lead-Free double perovskites Rb_2TlSbX_6 (X = Cl, Br, and I) as an emerging aspirant for solar cells and green energy applications, Sol. Energy 279 (Sep. 2024) 112844, https://doi.org/10.1016/J.SOLENER.2024.112844.

[87] N. Xu, et al., First-principles study on the structure, mechanical, electrical, optical, kinetic, thermodynamic and hydrogen storage properties of the hydride perovskites $XScH_3$ (X = K, Rb, Cs) for hydrogen storage applications, J. Energy Storage 107 (Jan. 2025) 114945, https://doi.org/10.1016/J.EST.2024.114945.

[88] A. Ayyaz, et al., A comprehensive DFT exploration of physical characteristics of halide double perovskites $Na_2AgGa(Cl/Br)_6$: Environment-Friendly alternatives for renewable energy technologies, Inorg. Chem. Commun. 170 (Dec. 2024) 113291, https://doi.org/10.1016/J.INOCHE.2024.113291.

[89] S. Lee, et al., Giant magneto-elastic coupling in multiferroic hexagonal manganites, Nature 451 (7180) (Feb. 2008) 805–809, https://doi.org/10.1038/NATURE06507;KWRD=SCIENCE.

[90] A. Ayyaz, et al., Unveiling theoretical findings on optoelectronic and transport characteristics of $Na_2ScAu(Cl/Br/I)_6$ for energy conversion applications, Opt. Quant. Electron. 57 (6) (Jun. 2025) 1–24, https://doi.org/10.1007/S11082-025-08282-1, 2025 57:6.

[91] M. Tarekuzzaman, et al., Analyzing the physical properties of Half-heusler RNiSb (R = Sc, Y) for optoelectronic and thermoelectric applications based on first-principles theories, Phys. Scripta 99 (10) (Sep. 2024) 105920, https://doi.org/10.1088/1402-4896/AD729A.

[92] Z. Wang, S. Tao, J. Deng, H. Zhou, Q. Yao, Significant improvement in the dehydriding properties of perovskite hydrides, $NaMgH_3$, by doping with K_2TiF_6, Int. J. Hydrogen Energy 42 (12) (Mar. 2017) 8554–8559, https://doi.org/10.1016/J.IJHYDENE.2016.12.078.

[93] M. Usman, et al., First-principles calculations to investigate structural, electronics, optical, and mechanical properties of Bi-based novel fluoroperovskites $TBiF_3$ (T = Hg, Xe) for optoelectronic applications, Mater. Sci. Semicond. Process. 160 (Jun. 2023) 107399, https://doi.org/10.1016/J.MSSP.2023.107399.

[94] D.Y. Hu, X.H. Zhao, T.Y. Tang, L. Li, Y.L. Tang, Insights on structural, elastic, electronic and optical properties of double-perovskite halides Rb_2CuBiX_6 (X=Br, Cl), J. Phys. Chem. Solid. 167 (Aug. 2022) 110791, https://doi.org/10.1016/J.JPCS.2022.110791.

[95] M.M. Parvaiz, A. Khalil, H.I. Elsaeedy, M.B. Tahir, S. Ayub, Z. Ullah, Extensive screening of novel $BaXH_3$ (X = V, Cr, Co, Ni, Cu, and Zn) perovskites for physical properties and hydrogen storage application: a DFT study, Int. J. Hydrogen Energy 87 (Oct. 2024) 1056–1073, https://doi.org/10.1016/J.IJHYDENE.2024.09.113.

[96] M. Manzoor, et al., Probing direct bandgap of double perovskites Rb_2LiTlX_6 (X = Cl, Br) and optoelectronic characteristics for solar cell applications: DFT calculations, J. Mater. Res. Technol. 18 (May 2022) 4775–4785, https://doi.org/10.1016/J.JMRT.2022.04.073.

[97] J. Yu, S. Chen, Y. Chen, J. Hou, S. Li, Z. Shi, First-principles study of structural, elastic, electronic and optical properties of cubic perovskite $AgXF_3$ (X = Be, Mg, Ca and Sr) compounds, Mater. Today Commun. 34 (Mar. 2023) 105258, https://doi.org/10.1016/J.MTCOMM.2022.105258.

[98] A. Rafique, M. Usman, J.U. Rehman, A. Nazeer, H. Ullah, A. Hussain, Investigation of structural, electronic, mechanical, optical and hydrogen storage properties of cobalt-based hydride-perovskites $XCoH_3$ (X = In, Mn, Sr, Sn, Cd) for hydrogen storage application, J. Phys. Chem. Solid. 181 (Oct. 2023) 111559, https://doi.org/10.1016/J.JPCS.2023.111559.

[99] Q. Ain, et al., A precise prediction of structure stability and hydrogen storage capability of $KCdH_3$ perovskite hydride using density functional theory calculations, J. Energy Storage 100 (Oct. 2024) 113734, https://doi.org/10.1016/J.EST.2024.113734.

[100] M. Ali, Z. Bibi, M. Mubashir, M.W. Younis, U. Afzal, A. El-marghany, A computational investigation of lithium-based metal hydrides for advanced solid-state hydrogen storage, ChemistrySelect 9 (10) (Mar. 2024) e202304582, https://doi.org/10.1002/SLCT.202304582.

[101] B. Ahmed, et al., An Ab-initio simulation of boron-based hydride perovskites XBH_3 (X = Cs and Rb) for advance hydrogen storage system, Comput. Theor. Chem. 1225 (Jul. 2023) 114173, https://doi.org/10.1016/J.COMPTC.2023.114173.

[102] Y. Du, et al., First-principles study of the hydrogen storage properties of hydride perovskites $XCuH_3$ (X = K, Rb) for hydrogen storage applications, Int. J. Hydrogen Energy 78 (Aug. 2024) 713–720, https://doi.org/10.1016/J.IJHYDENE.2024.06.352.

[103] Q. Zeng, K. Su, L. Zhang, Y. Xu, L. Cheng, X. Yan, Evaluation of the thermodynamic data of CH_3SiCl_3 based on Quantum chemistry calculations, J. Phys. Chem. Ref. Data 35 (3) (Sep. 2006) 1385–1390, https://doi.org/10.1063/1.2201867.

[104] A. Bakar, et al., Investigations for hydrogen storage applications of $XPtH_3$ (X = Cs, Fr) hydrides: a first principles study, Chem. Phys. 591 (Mar. 2025) 112566, https://doi.org/10.1016/J.CHEMPHYS.2024.112566.
[105] A. Waqdim, et al., Lithium-based hydride perovskites $LiXH_3$ (X = Mo, Tc, Rh) for hydrogen storage applications: a DFT study, Int. J. Hydrogen Energy 153 (Jul. 2025) 150065, https://doi.org/10.1016/J.IJHYDENE.2025.150065.
[106] A. Bakar, H. Muhammad, A. Afaq, G.K. Toleubay, E.O. Shalenov, H.E. Ali, ab-initio insights of $BeXH_3$ (X=In,Sn,Sb) hydrides for structural, phonon, electronic, thermodynamic and hydrogen storage properties, J. Energy Storage 132 (Oct. 2025) 117817, https://doi.org/10.1016/J.EST.2025.117817.